Solar Energy Materials & Solar Cells 263 (2023) 112585

Contents lists available at ScienceDirect

Solar Energy Materials and Solar Cells

journal homepage: www.elsevier.com/locate/solmat

Optimization of efficiency enhancement of TOPCon cells with boron selective emitter

Xinlu Li [a], QinQin Wang [b], Xu Dong [b], Jiadong Li [b], XinYu Zhang [c], Ningyi Yuan [a,*], Lvzhou Li [b,**], Jianning Ding [a,b,d,***]

[a] School of Materials Science and Engineering, Jiangsu Collaborative Innovation Center for Photovoltaic Science and Engineering, Jiangsu Province Cultivation Base for State Key Laboratory of Photovoltaic Science and Technology, Changzhou University, Changzhou, 213164, Jiangsu, PR China
[b] Institute of Technology for Carbon Neutralization, Yangzhou Technological Innovation Institute for Carbon Neutralization, Yangzhou University, Yangzhou, 225127, Jiangsu, PR China
[c] Jinko Solar Co., Ltd, Haining, 314400, Zhejiang, PR China
[d] Institute of Intelligent Flexible Mechatronics, Jiangsu University, Zhenjiang, 212013, PR China

ARTICLE INFO

Keywords:
Silicon solar cell
Tunnel oxide passivating Contact (TOPCon) structure
Selective emitter
Boron diffusion
Ag/Al paste

ABSTRACT

Silicon solar cells with a tunnel oxide passivating contact (TOPCon) structure are the new mainstream products; however, emitter recombination has become the bottleneck for further improvement. The introduction of selective emitter (SE) technology becomes imperative to address this issue. In this study, the appropriate range of sheet resistance in the light-doped region (230–280 Ω/sq)and the reasonable interval of the diffusion junction depth in the heavy-doped region (1.2–1.3 μm) are presented. The selective emitter with a suitable doping distribution is realized using the mask and etch-back method. Compared to the homogeneous emitter with a sheet resistance of 150 Ω/sq, J_{0e} of 16 fA/cm^2, and $J_{0metal\text{-}front}$ of 500 fA/cm^2, the optimum selective emitter results in a $J_{0e\text{-}light\ doping}$ of 8 fA/cm^2, $J_{0e\text{-}heavy\ doping}$ of 45 fA/cm^2 and $J_{0metal\text{-}front}$ of 213 fA/cm^2. Finally, the boron SE-TOPCon cell samples U_{OC} (726.5 mV), *FF* (84.01%), and efficiency (25.51%) are obtained, compared with the TOPCon cell with homogeneous emitter U_{oc} (717.6 mV), *FF* (83.77%) and efficiency (25.17%) of the reference. In addition, the efficiency potential of the boron SE-TOPCon cell (26.02%) at the optimal process conditions is determined based on device simulations. This study provides a feasible technical path for mass-produced TOPCon cells to increase the efficiency to more than 26%.

1. Introduction

Efficiency improvement and cost reduction are the two main goals in the photovoltaic manufacturing industry. Passivated emitter and rear (PERC) cells constitute more than 80% of the market share of mainstream photovoltaic products. However, the mass-production efficiency of PERC cells is 23.5–24% [1,2], and there is little room for further improvement. After PERC cells, there are two technical routes, tunnel oxide passivating contacts (TOPCon) and heterojunction with intrinsic thin-film (HJT) cells, whose theoretical efficiencies are 28.7% and 28.5%, respectively [3–5]. At present, TOPCon has become the primary choice for the next generation of mass-production products owing to its low cost of upgrading equipment and high compatibility with traditional PERC cell production lines [6–8]. Furthermore, the conversion efficiency of industrial TOPCon cells is above 25%. The reduction of the emitter dark saturation current density (J_{0e}) and the recombination losses under metal contact (J_{0metal}) in the emitter is crucial to improving the conversion efficiency of TOPCon cell [9,10]. The introduction and development of a boron selective emitter (SE) can increase the efficiency of a TOPCon cell.

Currently, boron doping mainly adopts low-pressure boron diffusion, typically divided into four steps: ①pre-oxidation, ②deposition of boron sources, ③drive-in, and ④post-oxidation [11]. Because of not using the boron SE process, the sheet resistance of TOPCon cells front boron

* Corresponding author.
** Corresponding author.
*** Corresponding author. School of Materials Science and Engineering, Jiangsu Collaborative Innovation Center for Photovoltaic Science and Engineering, Jiangsu Province Cultivation Base for State Key Laboratory of Photovoltaic Science and Technology, Changzhou University, Changzhou, 213164, Jiangsu, PR China.
E-mail address: nyyuan@cczu.edu.cn (N. Yuan).

https://doi.org/10.1016/j.solmat.2023.112585
Received 8 July 2023; Received in revised form 24 September 2023; Accepted 28 September 2023
Available online 1 October 2023

diffusion is 140–150 Ω/sq. The boron diffusion depth of TOPCon cells without a SE structure typically ranges from 0.7 to 1.2 μm, whereas the maximum spike depth of the screen-printed AgAl paste can extend up to 1.8 μm [12]. This also suggests that the paste is likely to permeate the PN junction, which results in a high J_{0metal} > 500 fA/cm^2 [13,14]. Silver-aluminum spikes only begin to significantly affect J_0 within the "key region" of 150 nm in the vicinity of the PN junction boundary, which generally corresponds to doping concentrations larger than 1 × 10^{18} atom/cm^3 [12](the "heavy doped depths" and "junction depths" in the study all refer to platform depths > 1 × 10^{18}). Therefore the effect of heavy doped depths on the front J_{0metal} in boron SE-TOPCon cells is significant.

Solutions such as selective laser doping (laser boron SE), the mask and etch-back method, and double boron diffusion can achieve boron SE structure. Among them, laser boron SE is widely used in the industry and is based on the boron diffusion process where additional local doping is performed by laser after the drive-in step; then, a high-temperature post-oxidation is implemented to form a lightly doped zone. The advantage of laser boron SE is the simplicity of the process and the efficiency gains of 0.2–0.3% [15,16]. However, the heavily doped zone formed by laser boron SE has a higher dopant concentration of B atoms. In contrast, the surface concentration of B atoms is only equal to that of the lightly doped zone after the post-oxidation step (>1000 °C, equivalent to step ④ of boron diffusion). Hence, the heavy doping zone cannot be matched to paste with a low aluminum content.

This study adopts the mask and etch-back method to achieve the boron SE structure. This method requires only one-time boron diffusion and does not require a laser. Furthermore, the method has cost advantages compared to the laser boron SE scheme, can address the low surface concentration of the heavy doping zone, and can expand the gap of doping amount between the light and heavy doping zones. However, the heavy doping depth in this scheme and the reasonable window of the light doping with needed sheet resistance need to be clarified. To address these problems, we analyzed the mass production data of a boron SE structure achieved using the mask and etch-back method and proposed an optimization scheme. The appropriate sheet resistance in the light doping zone and the optimum range of the junction depth in the heavy doping zone were determined. Using the optimized boron SE, the batch cell efficiency can achieve a gain of 0.3–0.4%.

2. Experimental details

2.1. Sample fabrication

The methodology for preparing experimental samples is illustrated in Fig. 1a. Samples A1-A10 were prepared by modifying the boron diffusion process to achieve varying junction depths, in order to examine the impact of junction depth on J_{0metal}. Samples B1-B6 were fabricated as double-sided boron diffusion samples with diverse sheet resistances in order to examine the correlation between J_{0e} and doping level. Fig. 1b illustrates the schematic diagram depicting the structure of the BSE cell sample. Samples C1-C3 were utilized as cell samples shows in Fig. 1b to evaluate the impact of boron diffusion concentration and junction depth on the Fill Factor (*FF*) performance of the cell. In the experiment, N-type monocrystalline silicon wafers with a resistivity ranging from 1 to 5 Ω cm and dimensions of 182 mm × 182 mm × 0.13 mm were utilized. A mixed solution of KOH and H_2O_2 was used to clean the wafers, and a pyramidal morphology of a height of ~3 μm was then formed on the surface during the texturing process in the KOH solution. Boron diffusion was conducted in a low-pressure thermal diffusion furnace using BCl_3 gas. To prepare the samples used for testing minority carrier lifetime, BSG was removed by using 30% HF solution for 1 min, followed by 3–5 nm Al_2O_3 deposition using atomic layer deposition (ALD) equipment. A tubular plasma-enhanced chemical vapor deposition (PECVD) device deposited a 70–100 nm SiNx-SiOx composite film and fired after PECVD deposition to activated surface passivation. To prepare cell samples, the rear side undergoes alkaline etching using an 80 °C KOH solution to achieve a reflectance of over 30%. Subsequently, low-pressure chemical vapor deposition (LPCVD) and low-pressure phosphorus diffusion were used to prepare the Poly-Si on oxide (POLO) structure on the rear side. After removing the front polysilicon and surface film layers using HF etching combined with alkali etching, the front side Al_2O_3 and SiNx-SiOx composite films were prepared. Then 80–90 nm thick SiNx films were deposited on the rear side of the cell samples using PECVD equipment, and the contact was formed using printing sintering of the Ag/Al paste for front-side metallization and Ag paste for rear-side metallization.

(1) To compare the influence of junction depth on J_{0metal}, ten double-sided boron diffusion samples with different junction depths (the "junction depths" in the study all refer to platform depths > 1 × 10^{18}) of 0.58, 0.71, 0.80, 0.84, 0.91, 0.94, 0.98, 1.09, 1.21, and

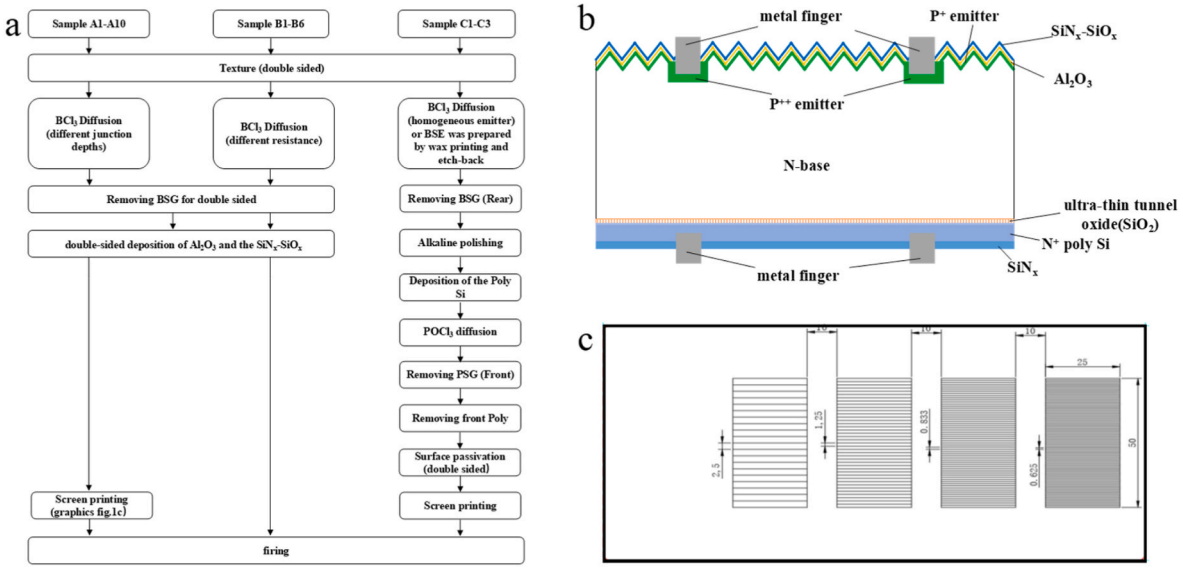

Fig. 1. (a) Preparation process diagram of samples; (b) Schematic diagram of TOPCon cell with SE technology; (c) J_{0metal} test graphics.

1.43 μm were prepared, and named as A1-A10, respectively. Then, the double-sided BSG was removed, followed by the double-sided deposition of Al_2O_3 and the SiNx/SiOx passivation layer. Subsequently, single-side metal contact was conducted, as shown in Fig. 1c. The relationship between PL and J_0 was calculated through the grid-free line zone, and the changes of different metalized zones corresponding to dark saturation current density (J_0) were tested. The linear relationship was fitted to obtain J_{0metal} [17,18].

(2) To investigate the influence of the sheet resistance of the light doping zone on implied open-circuit voltage (iV_{oc}), five double-sided boron diffusion samples with different sheet resistances of 100, 150, 200, 250, 300, and 400 Ω/sq were prepared, and named as B1-B6, respectively. Then, the double-sided BSG was removed, followed by the double-sided deposition of Al_2O_3 and the SiN_x/SiO_x passivation layer.

(3) Boron SE structure cell samples named C1-C3 were prepared using the mask and etch-back method (employs wax as the masking material, utilizing printing to achieve localized deposits). After completing the boron diffusion process, the wax layer is applied by printing method to protect the heavily doped area. The buffer oxide etching solution (BOE) with a volume ratio of NH_4F to HF of 7:1 was used to etch the lightly doped region at 21 °C, ensuring that the thinning was controlled in the range of 0.3–0.8 μm, while maintaining the pyramid structure of the wafer surface. The cell structure is shown in Fig. 1b. After texture preparation, the lightly and heavily doped zones of boron diffusion were completed. The emitter of C1 adopted the boron diffusion process with a sheet resistance of 130 Ω/sq. In addition, the boron SE structure was applied to C2 and C3. The sheet resistance in the light and heavy doping regions of C2 were 191 and 102 Ω/sq, respectively (the heavily doped region has the same peak concentration as C1, however, different junction depth). The lightly doped region of C3 was similar to that of C2, while its heavily doped region had a sheet resistance of 145 Ω/sq (same junction depth as C1, however, different peak concentration).

2.2. Characterization

The current-voltage (open-circuit voltage U_{oc}, short-circuit current density J_{sc}, fill factor *FF*, and conversion efficiency η) parameters were measured using a Halm tester calibrated using a Fraunhofer Institute for solar energy systems (ISE) standard cell. The iV_{oc} values of the controlled samples were determined using a lifetime tester at an illumination of 1 sun (WCT-120 Sinton, Boulder, CO, USA). The samples' passivated J_{0e} and J_{0metal} values were measured using the WCT-120 Sinton tester and extracted at an excess carrier density of 3×10^{15} cm^{-3} [19,20]. The B-doped profiles of the monitor wafers were measured by the electrochemical capacitance-voltage (ECV) device (WEP CVP21) using a 0.1 M NH_4F solution as the etchant (The surface factor of the measurement spot was calibrated by employing ECV testing and performing sheet resistive fitting). The specific contact resistivity (ρ_c) of the screen-printed metalized contact with different profiles was determined by the transfer length method (TLM) (GP-4 TEST) [21].

2.3. Simulation

Quokka (version 2.2.5, manufacturer, location) was used to simulate cell devices. Boron's SE structure was used on the front side (conventional TOPCon structure required the same parameters in the SE region and light-doped zone). The related parameters measured in the mass-production experiment were substituted into the device simulation to confirm the corresponding improvement effect of each processing window.

3. Results and discussion

3.1. Determining the appropriate boron diffusion junction depth

Boron diffusion samples with different junction depths (A1-A10) were prepared based on process debugging. The doping profile is shown in Fig. 2a, and the junction depths were 0.58, 0.71, 0.80, 0.84, 0.91, 0.94, 0.98, 1.09, 1.21, and 1.43 μm for A1-A10, respectively.

The J_{0metal} data for different junction depths are listed in Table 1. With the increase in junction depth, J_{0metal} decreased gradually; however, J_{0e} increased gradually, and the total dark saturation current density in the heavily doped region ($J_{0total\text{-}heavy\ doped}$) reached the limit gradually.

$$J_{0total-heavy\ doped} = J_{0metal} \times \frac{\text{metal print widths}}{\text{heavily doped widths}} + J_{0e} \times \left(1 - \frac{\text{metal print widths}}{\text{heavily doped widths}}\right) \quad (1)$$

Based on the current industrial mass-production conditions of the TOPCon cell, the simulation calculation is conducted under the condition that the metal printing finger lines and heavily doped finger lines have respective widths of 25 and 100 μm (the heavily doped gate area encompasses the metal printing gate area). The $J_{0total\text{-}heavy\ doped}$ as a function of junction depth is shown in Fig. 2b. When the junction depth exceeded 1.1 μm, the decline of $J_{0total\text{-}heavy\ doped}$ began to slow down. At this time, J_{0e} was still increasing gradually. When the junction depth of boron diffusion reached ~1.2 μm, the $J_{0total\text{-}heavy\ doped}$ in the heavily doped zone reached a minimum of ~95 fA/cm^2. The optimum condition is that the junction depth ranges from 1.2 to 1.3 μm.

3.2. Influence of sheet resistance of light doping zone on J_0

The boron diffusion doping profile of the cell with homogeneous emitter is represented by sample B2 in Fig. 3a. Its surface concentration was controlled at $\sim 9 \times 10^{18}/cm^2$, the junction depth was in the range of 0.75–0.8 μm and after the passivation the J_{0e} was 16–20 fA/cm^2, and iV_{oc} was 705–710 mV.

The iV_{oc} and J_0 results for B1-B6 are shown in Fig. 3b, where iV_{oc} is the measured result of WCT120, and J_0 is the calculated result (single surface J_0). J_0 gradually decreased as a function of sheet resistance; however, the upward trend was not linear. As the sheet resistance increased, its influence on J_0 gradually weakened. The sheet resistance of sample B2 was 150 Ω/sq, representing the recombination level of the boron-diffused emitter on the front of TOPCon solar cells, and the J_0 of sample B2 was 20 fA/cm^2. The J_0 of sample B3 decreased from 20 to 15 fA/cm^2 as sheet resistance increased from 150 to 200 Ω. The lower J_0 under the passivation layer benefits from a low peak concentration and a shallow junction. The sheet resistance of sample B5 increased to 300 Ω/sq, and J_0 decreased by 2.7 fA/cm^2 compared with sample B3. At this point, the downward trend of the J_0 is no longer significant as the sheet resistance further increases.

3.3. Effect of lateral transmission and contact resistivity on Fill Factor

It is known that boron diffusion with high-sheet resistance can effectively reduce the Auger recombination and J_{0e}. However, considering the increase in the contact and lateral resistances, the fill factor (*FF*) will decrease as the sheet resistance increases. To study the effect of the doping profile on cell *FF*, C1~C3 were prepared using the mass production grids (finger width of 25 μm and pitch of 1359 μm). The diffusion profile is shown in Fig. 4a, and the results are shown in Fig. 4b and c.

Fig. 4b and c shows measured heavy doping sheet resistance and contact resistivity, respectively. The sheet resistance of the metal contact zone of C1 and C2 is 130 and 102 Ω/sq, respectively. The sheet

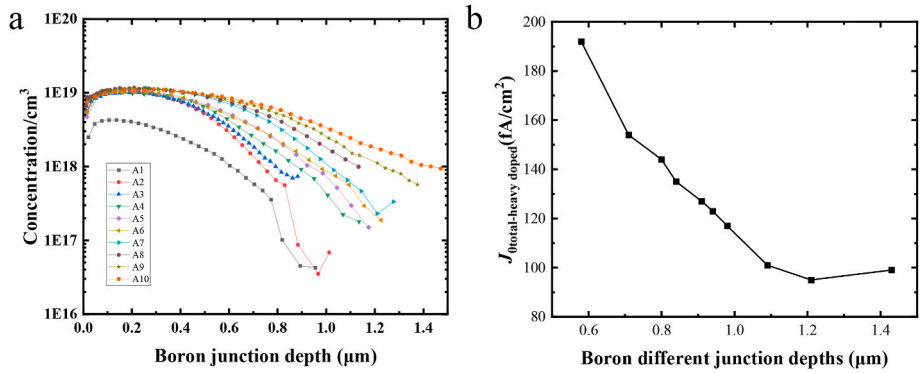

Fig. 2. (a) Doping profile with different heavy doping; (b) Correspondence between J_{0total} and heavy doping depths.

Table 1
Verification results of boron diffusion sample J_{0metal} with different junction depths.

Sample	Junction depths (μm)	Sheet resistance Ω/sq	J_{0metal} (fA/cm^2)	J_{0e} (fA/cm^2)	$J_{0total\text{-}heavy\ doped}$ (fA/cm^2)
A1	0.58	274	734	12	192
A2	0.71	143	564	18	154
A3	0.80	137	521	18	144
A4	0.84	124	475	21	135
A5	0.91	116	436	24	127
A6	0.94	110	401	31	123
A7	0.98	98	358	37	117
A8	1.09	90	268	46	101
A9	1.21	78	213	56	95
A10	1.43	63	194	68	99

resistance difference of 28 Ω/sq is due to the different diffusion depths of the two samples. Compared with sample C1, the ρ_c of sample C2 decreased by 0.41 mΩ cm^2. The peak concentration difference between sample C1 and C3 resulted in only 15 Ω/sq sheet resistance deviation; however, the effect of ρ_c was evident, and the difference reached 1.7 mΩ cm^2. According to the results, ρ_c can be reduced by increasing the boron diffusion profile's junction depth and peak concentration. There are similar reports in relevant literature regarding the relationship between ρ_c and peak concentration [22]. At similar sheet resistance gradients, the difference in peak concentration significantly influences the ρ_c.

The electrical properties of C1, C2, and C3 are shown in Table 2. As shown in Fig. 4c, the ρ_c of samples C1 and C2 is close. The main difference is that the sheet resistance of light doping region in sample C2 reaches 200 Ω/sq much higher than that in sample C1 (130 Ω/sq). Analysis of the *IV* data shows a 0.6% lower *FF* when sample C2 has a 7 mV U_{oc} advantage compared with sample C3. This is most likely a loss due to the lateral resistance.

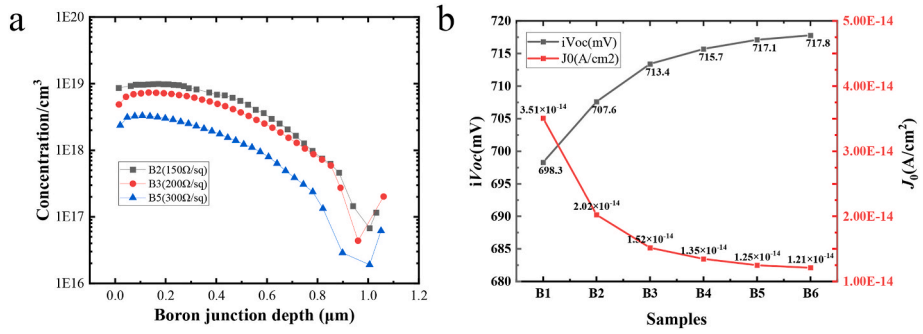

Fig. 3. (a) Existing boron diffusion profile; (b) iV_{oc} results after passivation of symmetrical structures with different boron diffusion resistance.

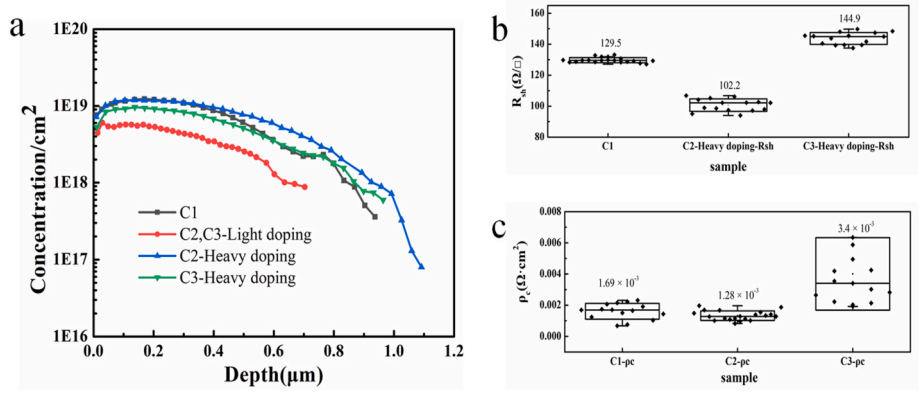

Fig. 4. (a) Light and heavy doping diffusion profile; (b) Comparison of measured heavy doping sheet resistance; (c) Measured contact resistivity.

Table 2
Comparison results of solar cell samples with and without boron SE.

Sample	η (%)	U_{oc} (V)	J_{sc} (mA/cm^2)	*FF* (%)	R_{ser}(mΩ·cm^2)
C1(BL)	24.71	0.7139	41.17	84.01	16.22
C2(BSE-1)	24.33	0.7214	40.41	83.41	24.30
C3(BSE-2)	23.92	0.7162	40.22	83.09	41.81

From the results of sample C3, *FF* was reduced by 0.3% based on sample C2, and their lightly doped sheet resistance was the same, which indicates that their lateral resistance loss was consistent. Therefore, the difference between C2 and C3 is due to the difference in ρ_c. Combining the relationship of J_0 and sheet resistance, the sheet resistance of the lightly doped boron SE structure needs to be higher than 200 Ω/sq to decrease J_0. In contrast, the ρ_c advantage introduced by the peak concentration in the heavily doped region cannot compensate for the *FF* loss caused by the lateral resistance. The decrease in J_{sc} of C2 and C3 is likely attributable to the softening of the pyramid morphology on the surface of the wafer. This softening, in turn, results in an enhanced surface reflectance during the etching process using BOE solution.

3.4. Cell structure simulations

The simulated open-circuit voltage U_{oc} of the SE structure is shown in Table 3. The result indicates that U_{oc} of the boron SE structure can be increased by nearly 10 mV at the optimal mass production window.

When the parameters of the TOPCon cell with homogeneous emitter whose efficiency reached 25.18% (the standard mass production level) were imported, power loss was calculated as shown in Table 4. As shown in Table 4, when a dense grid (the proportion of metal area on the front of the cell increased from 1.8 to 1.95%) was introduced into the cell with homogeneous emitter, it can be concluded that the increase in *FF* does not compensate for the loss of J_{sc} and U_{oc}. The front J_{0e} and J_{0metal} are the primary factors contributing to the loss of efficiency, and the main purpose of SE technology was to optimize this problem. The lower J_{0metal} of the boron SE-TOPCon cell means that it can match denser meshes, and the *FF* significantly increased, which can effectively compensate for the loss of U_{oc} and J_{sc} and achieve improved efficiency.

To investigate the influence of the boron SE-TOPCon cell parameters on the efficiency improvement, we take the cell with homogeneous emitter which achieves an efficiency of 25.18% as a baseline, and then we calculate the impact of the different settings as shown in Table 5. By only reducing J_{0e} or $J_{0,metal}$, leaving other parameters unchanged, the efficiency increases by 0.31% and 0.13%, respectively. In addition, we only increase the sheet resistance of emitter from 150 to 250 Ω/sq, or decrease ρ_c from 1.3 to 0.8 Ω cm^2, the change in cell efficiency (−0.12% and 0.05%, respectively) are also listed in Table 5.

Based on the analysis of Tables 5 and it can be seen that J_{0e} in the light-doped area and J_{0metal} in the heavily-doped area crucial to improve the efficiency of the boron SE-TOPCon cell. In contrast, lateral transmission and front finger line shading are the deficiencies that impact cell efficiency improvement.

Table 3
The calculated U_{oc} of the TOPCon cells with boron SE and homogeneous emitter.

	Boron-SE	Homogeneous emitter
Light doping J_{0e} (fA/cm^2)	8.0	16.0
Heavy doping J_{0e} (fA/cm^2)	45.0	
Front J_{0metal} (fA/cm^2)	213.3	510.0
Front metal proportion	1.81%	1.81%
Heavy doping proportion	5.44%	0.00%
Rear J_{0pass} (fA/cm^2)	1.0	1.0
Rear J_{0met} (fA/cm^2)	65.0	65.0
Rear metal proportion	2.37%	2.37%
J_{0bulk} (fA/cm^2)	10.0	10.0
$J_{0total\text{-}front}$ (fA/cm^2)	15.2	25.0
$J_{0total\text{-}rear}$ (fA/cm^2)	2.5	2.5
J_{0total} (fA/cm^2)	27.7	37.5
J_{sc} (mA/cm^2)	41.30	41.37
U_{oc} (V)	0.7272	0.7189

3.5. Realization of process window

Different from the preparation of C group, this section of cell group combined with previous experiments to explore the process window and process plan, this study adopted the wax print and etch-back method to achieve the boron SE-TOPCon cell and the superimposed screen pattern optimization to improve the *FF* defects for cell efficiency verification. Compared with the cell with homogeneous emitter, the efficiency was improved by 0.36%, and the combined SE cell efficiency reached 25.51% (see Table 6).

The improvement of cell efficiency was due to the increase of U_{oc} to 9 mV; this finding is consistent with the calculated results. In addition, *FF* increased significantly after the SE structure was introduced into the dense gate (part of U_{oc} gain is given up). The J_{sc} of the boron SE group was lower than that of BSL, caused by the shading loss in the heavily doped zone. Compared with the tested *EQE* of cell, the advantage of the blue light response brought by the low concentration of the shallow junction in the light-doped zone can balance this problem; however, introducing a dense gate still leads to the reduction of current.

The experimental platform used for this study is the TOPCon half-piece cell mass production line. The finger width used for screen printing of mass production line is 25 μm, whereas the width of the finger can be 12 μm using the plating technology [23,24] Stacking a 12 μm finger width on the front of the boron SE-TOPCon cell improves efficiency by 0.3%. Reducing the finger width decreases the front finger shading, and also reduces the fraction of J_{0metal} in the J_{0total}, thus improving the U_{oc}. At this time, the U_{oc} of the cell has reached 730 mV, and with the decrease of the finger width, the width of the heavily doped region can also be reduced to 50 μm, and the U_{oc} is further increased by 2 mV. Under the condition of the fingers with 12 μm width, the grid density was again optimized (2.23% metal region), which increased *FF* by 0.4%. In this study, the minority carrier lifetime of N-type monocrystalline silicon wafers is shorter than 500 μs, which is not the best level in the industry. The bulk life, set as 1 ms, was substituted into the optimized boron SE-TOPCon cell model for simulation calculation. Finally, the 26% efficiency potential of the boron SE-TOPCon cell can be reached under mass production conditions, as shown in Fig. 5.

4. Conclusions

This study has demonstrated that the appropriate range of sheet resistance in the light-doped region is 230–280 Ω/sq, and the reasonable interval of diffusion junction depth in the heavy-doped region is 1.2–1.3 μm. The boron SE TOPCon cell with suitable doping distribution is realized using the wax print and etch-back method, achieving an efficiency increase higher than 0.3%, compared with cell with homogeneous emitter (whose efficiency is 25.17%).

The simulation results show that the change in efficiency by including J_{0e}, front $J_{0metal,}$ and ρ_c in the boron SE-TOPCon cell structure is 0.31%, 0.13%, and 0.05%, respectively. The high lateral resistance caused by light doping is larger than 200 Ω/sq results in a 0.12% efficiency reduction. The main reasons for the power loss of the cell are the front finger shading and lateral resistance. Stacking 12 μm finger width on the front of a boron SE-TOPCon cell improves efficiency by 0.3%. Then, the width of the heavily doped region is reduced to 50 μm, and the efficiency is again enhanced by 0.07%. In this way, the efficiency of the cell reaches 25.9%. Additionally, the grid density is optimized under conditions of 12 μm finger width, and using the existing market silicon wafer with a high minority carrier lifetime (>1 ms), the simulated cell efficiency reaches 26.02%. This study provides the efficiency improvement path and scale process route for TOPCon cells.

Table 4
Power loss simulation results of the TOPCon cell with homogeneous emitter, the homogeneous emitter-based TOPCon cell with an optimized dense grid design, the BSE-TOPCon cell and the BSE-TOPCon cell with an optimized dense grid design.

		With homogeneous emitter	With homogeneous emitter and dense grid	With BSE	With BSE and dense grid
η (%)		25.18	25.14	25.53	25.56
U_{oc} (mV)		718.2	717.6	729.1	728.3
J_{sc} (mA/cm^2)		41.81	41.74	41.93	41.80
FF (%)		83.86	83.95	83.51	83.97
Sum optical (%)		0.483	0.532	0.388	0.469
Sum recombination	Bulk recombination (%)	0.224	0.219	0.250	0.238
	Emitter recombination (%)	0.485	0.466	0.215	0.196
	Front contact recombination (%)	0.247	0.275	0.107	0.142
	Rear contact recombination (%)	0.088	0.086	0.142	0.134
	Rear passivation recombination (%)	0.045	0.044	0.073	0.069
	Selective emitter recombination (%)	\	\	0.053	0.069
	Synergy recombination (%)	0.739	0.071	0.357	0.386
Sum resistance (%)		0.258	0.224	0.483	0.327

Table 5
The influence of the boron SE-TOPCon cell parameters on the efficiency improvement.

Sample	η (%)	U_{oc} (V)	J_{sc} (mA/cm^2)	*FF* (%)	$\triangle\eta$ (%)
homogeneous emitter	25.18	0.7182	41.81	83.86	\
J_{0e}	25.49	0.7254	41.80	84.04	0.31
J_{0metal}	25.31	0.7221	41.81	83.84	0.13
sheet resistance of emitter	25.06	0.7179	41.82	83.47	−0.12
ρ_c	25.23	0.7182	41.81	84.01	0.05

Table 6
Results of TOPCon cell with boron SE structure.

Sample	η (%)	U_{oc} (V)	J_{sc} (mA/cm^2)	*FF* (%)
E1(TOPCon)	25.17	0.7176	41.87	83.77
E2(BSE-TOPCon)	25.51	0.7265	41.83	84.01

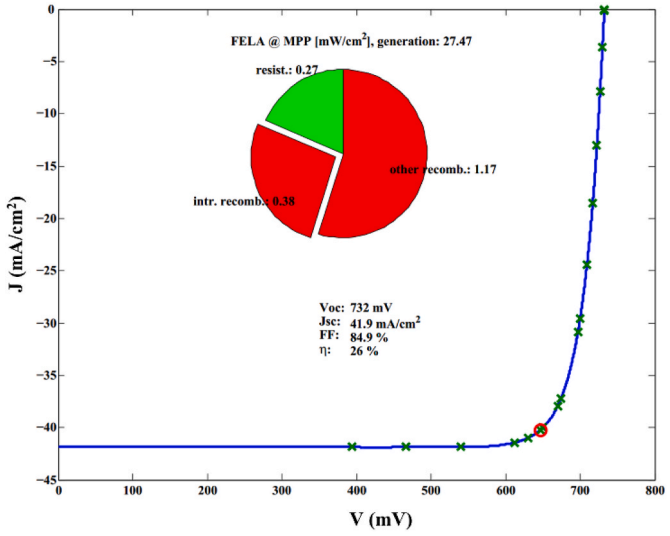

Fig. 5. Efficiency potential of BSE-TOPCon cell under mass production conditions.

CRediT authorship contribution statement

Xinlu Li: Methodology, Investigation. **QinQin Wang:** Investigation. **Xu Dong:** Validation, Investigation. **Jiadong Li:** Investigation. **XinYu Zhang:** Formal analysis. **Ningyi Yuan:** Writing – review & editing, Supervision, Project administration. **Lvzhou Li:** Writing – review & editing, Formal analysis. **Jianning Ding:** Writing – review & editing, Supervision, Resources, Funding acquisition, Conceptualization.

Declaration of competing interest

The authors declare that they have no known competing financial interests or personal relationships that could have appeared to influence the work reported in this paper.

Data availability

Data will be made available on request.

Acknowledgment

This work has been partially supported by the Special Fund for Science and Technology Innovation of Jiangsu Province (Grants No. BE2022022-4).

References

[1] A. Blakers, Development of the PERC solar cell, IEEE J. Photovoltaics 9 (2019) 629–635, https://doi.org/10.1109/JPHOTOV.2019.2899460.
[2] S. Banerjee, S.S.A. Askari, M.K. Das, Effect of rear contact coverage and improvement of efficiency of crystalline p-Si solar cell compared to state of art PERC cell, IEEE Access 11 (2023) 34999–35006, https://doi.org/10.1109/ACCESS.2023.3264900.
[3] J. Schmidt, P. Robby, B. Rolf, Surface passivation of crystalline silicon solar cells: present and future, Sol. Energy Mater. Sol. Cell. 187 (2018) 39–54, https://doi.org/10.1016/j.solmat.2018.06.047.
[4] T.G. Allen, J. Bullock, X. Yang, A. Javey, S. De Wolf, Passivating contacts for crystalline silicon solar cells, Nat. Energy 4 (11) (2019) 914–928, https://doi.org/10.1038/s41560-019-0463-6.
[5] W. Long, S. Yin, F. Peng, M. Yang, L. Fang, X. Ru, M. Qu, H. Lin, X. Xu, On the limiting efficiency for silicon heterojunction solar cells, Sol. Energy Mater. Sol. Cell. 231 (2021), 111291, https://doi.org/10.1016/j.solmat.2021.111291.
[6] Y. Chen, D. Chen, C. Liu, Z. Wang, Y. Zou, Y. He, Y. Wang, L. Yuan, J. Gong, W. Lin, X. Zhang, Y. Yang, H. Shen, Z. Feng, P.J. Verlinden, Mass production of industrial tunnel oxide passivated contacts (i-TOPCon) silicon solar cells with average efficiency over 23% and modules over 345 W, Prog. Photovoltaics Res. Appl. 27 (2019) 827–834, https://doi.org/10.1002/pip.3180.
[7] M.A. Green, K. Emery, Y. Hishikawa, W. Warta, E.D. Dunlop, Solar cell efficiency tables (Version 45), Progress in Photovoltaics (2012), https://doi.org/10.1002/pip.2573.
[8] M. Fischer, M. Woodhouse, S. Herritsch, J. Trube, International Technology Roadmap for Photovoltaic (ITRPV). VDMA EV. https://itrpv.vdma.org/en/ueber-uns, 2021.
[9] P. Zheng, J. Yang, Z. Wang, L. Wu, H. Sun, S. Chen, Y. Guo, H. Xia, S.P. Phang, E.-C. Wang, J. Stuckelberger, H.C. Sio, X. Zhang, D. Macdonald, H. Jin, Detailed loss analysis of 24.8% large-area screen-printed n-type solar cell with polysilicon passivating contact, Cell Reports Physical Science 2 (10) (2021), 100603, https://doi.org/10.1016/j.xcrp.2021.100603.
[10] M. Hermle, F. Feldmann, M. Bivour, J.C. Goldschmidt, S.W. Glunz, Passivating contacts and tandem concepts: approaches for the highest silicon-based solar cell efficiencies, Appl. Phys. Rev. 7 (2) (2020), https://doi.org/10.1063/1.5139202.

[11] Q. Wang, K. Guo, L. Yuan, L. Li, H. Peng, B. Li, A. Wang, L. Zhang, W. Wu, J. Ding, N. Yuan, Boron tube diffusion process parameters for high-efficiency n-TOPCon solar cells with selective boron emitters, Sol. Energy Mater. Sol. Cell. 253 (2023), 112231, https://doi.org/10.1016/j.solmat.2023.112231.
[12] N. Wöhrle, E. Lohmüller, J. Greulich, S. Werner, S. Mack, Towards understanding the characteristics of Ag–Al spiking on boron-doped silicon for solar cells, Sol. Energy Mater. Sol. Cell. 146 (2016) 72–79, https://doi.org/10.1016/j.solmat.2015.11.032.
[13] Q. Wang, W. Wu, Y. Li, L. Yuan, S. Yang, Y. Sun, S. Yang, Q. Zhang, Y. Cao, H. Qu, N. Yuan, J. Ding, Impact of boron doping on electrical performance and efficiency of n-TOPCon solar cell, Sol. Energy 227 (2021) 273–291, https://doi.org/10.1016/j.solener.2021.08.075.
[14] P. Zhu, Y. Liu, C. Cao, J. Tian, A. Zhang, D. Wang, Low recombination firing-through al paste for n-type solar cell with boron emitter, Materials 14 (4) (2021) 765, https://doi.org/10.3390/ma14040765.
[15] W. Lin, D. Chen, C. Liu, Y. Wang, Y. He, Y. Zou, L. Yuan, J. Gong, Y. Yang, Z. Feng, Z. Liu, Z. Chen, Q. Xie, Z. Liang, Y. Chen, H. Shen, Green-laser-doped selective emitters with separate BBr3 diffusion processes for high-efficiency n-type silicon solar cells, Sol. Energy Mater. Sol. Cell. 210 (2020), 110462, https://doi.org/10.1016/j.solmat.2020.110462.
[16] D. Ding, Z. Du, R. Liu, C. Quan, J. Bao, D. Du, Z. Li, J. Chen, W. Shen, Laser doping selective emitter with thin borosilicate glass layer for n-type TOPCon c-Si solar cells, Sol. Energy Mater. Sol. Cell. 253 (2023), 112230, https://doi.org/10.1016/j.solmat.2023.112230.
[17] V. Shanmugam, T. Mueller, A.G. Aberle, J. Wong, Determination of metal contact recombination parameters for silicon wafer solar cells by photoluminescence imaging, Sol. Energy 118 (2015) 20–27, https://doi.org/10.1016/j.solener.2015.05.010.
[18] B. Hallam, B. Tjahjono, T. Trupke, S. Wenham, Photoluminescence imaging for determining the spatially resolved implied open circuit voltage of silicon solar cells, J. Appl. Phys. 115 (4) (2014), 044901, https://doi.org/10.1063/1.4862957.
[19] R.A. Sinton, A. Cuevas, Contactless determination of current–voltage characteristics and minority-carrier lifetimes in semiconductors from quasi-steady-state photoconductance data, Appl. Phys. Lett. 69 (17) (1996) 2510–2512, https://doi.org/10.1063/1.117723.
[20] R.A. Sinton, A. Cuevas, M. Stuckings, Quasi-steady-state Photoconductance, a New Method for Solar Cell Material and Device Characterization, Conference Record of the Twenty Fifth IEEE Photovoltaic Specialists Conference-1996, IEEE, 1996, pp. 457–460, https://doi.org/10.1109/PVSC.1996.564042.
[21] S. Guo, G. Gregory, A.M. Gabor, W.V. Schoenfeld, K.O. Davis, Detailed investigation of TLM contact resistance measurements on crystalline silicon solar cells, Sol. Energy 151 (2017) 163–172, https://doi.org/10.1016/j.solener.2017.05.015.
[22] E. Lohmüller, S. Werner, R. Hoenig, J. Greulich, F. Clement, Impact of boron doping profiles on the specific contact resistance of screen printed Ag-Al contacts on silicon, Sol. Energy Mater. Sol. Cells 142 (2015) 2–11, https://doi.org/10.1016/j.solmat.2015.04.039. S.
[23] A. Kraft, Plated Copper Front Side Metallization on Printed Seed-Layers for Silicon Solar Cells (Doctoral Dissertation, Dissertation, Albert-Ludwigs-Universität Freiburg, 2015, 2015, https://d-nb.info/111945252X/34.
[24] B. Grübel, G. Cimiotti, C. Schmiga, S. Schellinger, B. Steinhauser, A.A. Brand, M. Kamp, M. Sieber, D. Brunner, S. Fox, S. Kluska, Progress of plated metallization for industrial bifacial TOPCon silicon solar cells, Prog. Photovoltaics Res. Appl. 30 (6) (2022) 615–621, https://doi.org/10.1002/pip.3528.